Environmental Science and Pollution Research (2018) 25:19423–19435
https://doi.org/10.1007/s11356-018-2079-y

RESEARCH ARTICLE

The hierarchical porous structure bio-char assessments produced by co-pyrolysis of municipal sewage sludge and hazelnut shell and Cu(II) adsorption kinetics

Bing Zhao[1] · Xinyang Xu[1] · Fanqiang Zeng[1] · Haibo Li[1] · Xi Chen[1]

Received: 21 March 2018 / Accepted: 17 April 2018 / Published online: 4 May 2018

Abstract

The co-pyrolysis technology was applied to municipal sewage sludge (MSS) and hazelnut shell with alkaline activating agent K_2CO_3 under N_2 atmosphere. The innovative bio-char produced by co-pyrolysis had significant physical and chemical characteristics. The specific surface area reached 1990.23 m^2/g, and the iodine absorption number was 1068.22 mg/g after co-pyrolysis at 850 °C. Although hazelnut shell was a kind of solid waste, it also had abundant cellulose resource, which could contribute to porous structure of bio-char during co-pyrolysis with MSS and decrease total heavy metals contents of raw material to increase security of bio-chars. Meanwhile, the residual fractions of heavy metals in bio-char were above 92.95% after co-pyrolysis at 900 °C except Cd to prevent heavy metals digestion, and the bio-char presented significant immobilization behavior from co-pyrolysis technology. Moreover, the yield and the iodine absorption number of bio-chars under different process variables were analyzed, and it was confirmed that appropriate process variables could contribute the yield and the iodine absorption number of bio-char and prevent to etch pore structure excessively to collapse. The changes of surface functional groups and crystallographic structure before and after co-pyrolysis were analyzed by FTIR and XRD, respectively. The hierarchical porous structure of bio-char was presented by SEM and N_2 adsorption-desorption isotherm. The Cu(II) adsorption capacity of the bio-char was 42.28 mg/g after 24 h, and surface functional groups acted as active binding sites for Cu(II) adsorption. Langmuir model and pseudo-second-order model can describe process of Cu(II) adsorption well.

Keywords Co-pyrolysis · Alkaline activating agent · Porous structure · BCR sequential extraction · Cu(II) adsorption

Introduction

The number of municipal wastewater treatment plants increases gradually in recent years as urbanization accelerating. Municipal sewage sludge (MSS) is a kind of by-product generated from municipal wastewater treatment plants and contains numerous harmful substances, such as heavy metals (Fang et al. 2016), microorganisms (Fernando and Fedorak 2005) and eggs of parasitic organisms (Fytili and Zabaniotou 2008). Improper disposal of MSS will release contaminants to the environment including soil and water and threat to human health (Bondarczuk et al. 2016). However, MSS is also a species of potential bio-resource due to high content of organic matters (Wei et al. 2011). Therefore, it is very important to develop a proper technology to combine disposal and recycling at the same time.

Pyrolysis technology offers a practical and effective method for stabilization and resource utilization of sewage sludge at the same time (Chen et al. 2014). Pyrolysis will minimize the volume of sludge, kill microorganisms and eggs of parasitic organisms, and the organic matters will be converted into bio-char (Zhao et al. 2018). Potentially useful bio-oils and pyrolysis gas will be produced for reuse (Cao and Pawłowski 2012). In recent years, the bio-char has received extensive attentions due to its wide availability, low cost, and favorable physical/chemical surface characteristics for pollutants' removal. Especially, the previous study indicates that heavy metals in MSS can be transformed from weakly bound to stable state via pyrolysis process to ensure the security of application (Jin et al. 2016). Meanwhile, it is feasible that

Responsible editor: Guilherme L. Dotto

✉ Xinyang Xu
1510467@stu.neu.edu.cn

[1] School of Resources and Civil Engineering, Northeastern University, Shenyang 110819, China

adding other biomass as a kind of carbon source without heavy metals can further decrease the total content of heavy metals and the environmental risk for the land application.

Hazelnut shell is a kind of solid waste from hazelnut production. As biomass, hazelnut shell has above 40% cellulose (Hoşgün et al. 2017). Compared with wheat straw, olive bagasse, hazelnut shell has lower ash content in favor of retaining higher yield of bio-char (Bakisgan et al. 2009). Hazelnut shell also has abundant cellulose resource, which can be transformed to porous bio-char by pyrolysis as traditional wood. Thus, hazelnut shell is selected to co-pyrolysis with MSS to increase porous structure and environmental friendliness for bio-chars.

In order to increase specific surface area of the bio-char, chemical activation has been tried during pyrolysis simultaneously. Notably, chemical activation reagents have a strong impact on characteristics of the bio-char. The most widely used activation reagent includes zinc chloride ($ZnCl_2$), phosphoric acid (H_3PO_4), and potassium hydroxide/carbonate (KOH/K_2CO_3). K_2CO_3 played an important role in the development of porosity during pyrolysis. Tran et al. (2017) used golden shower with K_2CO_3 to produce activated carbon, and the activated carbon had 1846 m^2/g of Langmuir surface area. In the adsorption/desorption isotherms, micropore and mesopore structures of the activated carbon presented hysteresis loop. Okman et al. (2014) used grape seed with K_2CO_3 and KOH to produce activated carbon. The activated carbon with the highest surface area of 1238 m^2/g was obtained at 800 °C in K_2CO_3, while KOH produced the activated carbon with the highest surface area of 1222 m^2/g in at 800 °C. Furthermore, the chemical activation agents must play an environmentally friendly role in industrial and environmental applications. Compared with $ZnCl_2$, K_2CO_3 does not have heavy metals, and it is frequently used in food additives. Therefore, K_2CO_3 was used as chemical activation agent in this work.

In this work, co-pyrolysis of MSS and hazelnut shell can decrease the total heavy metals content of raw materials effectively and produce the eco-friendly bio-char. Hazelnut shell and alkaline-activating agent K_2CO_3 contribute to produce larger surface area for adsorption application. Different process variables were used to analyze impact trend of the yield and the iodine absorption number for bio-chars. The changes of surface functional group by co-pyrolysis were analyzed by Fourier transform infrared spectrometer (FTIR). X-ray diffraction (XRD) analysis was used to identify crystallographic structure of the bio-char sample. The micromorphology was observed by scanning electron microscope (SEM), N_2 adsorption-desorption isotherm, and specific surface area analysis to confirm hierarchical porous structure and remarkable specific surface area. In order to evaluate the risk of heavy metals in bio-char by co-pyrolysis, BCR sequential extraction of heavy metals was applied based on distribution of the chemical species. The adsorption experiments of the bio-char for Cu(II) were used to analyze adsorption capacity, equilibrium model, and kinetic model to assess adsorption application.

Experimental

Raw materials

The MSS was obtained from dewatering room of an urban municipal wastewater treatment plant in Liaoning Province, China. Activated sludge system was used as the secondary treatment to wastewater. The MSS was submitted to stabilization treatment by adding polyacrylamide 4 wt‰ and then dehydration. Hazelnut shell was solid waste produced by hazelnut production and air dried. Before pyrolysis, the MSS was heated at 105 ± 5 °C for 24 h to remove free water. The raw materials of MSS and hazelnut shell were milled before co-pyrolysis (diameter equal to 1 mm) and packed in sealed plastic bags in a desiccator for further use. The proximate and ultimate analyses of raw materials are shown in Table 1. The moisture, volatile matter, and ash content were measured according to the method of coal industry analysis in China (Chinese standard methods, GB/T 212-2008). The total carbon (C), hydrogen (H), nitrogen (N), and sulfur (S) contents of MSS were determined using the elemental analyzer (Elementar Analysensysteme GmbH, vario EL cube V 1.2.1).

The heavy metal element (Cu, Zn, Ni, Pb, Cr, and Cd) contents of MSS were measured by inductively coupled plasma (ICP) instrument (LEEMAN, Prodigy XP) according to Chinese standard methods (GB18918-2002) after digested by $HNO_3/HClO_4/HF$ (3:1:1) solution, as shown in Table 2.

Table 1 Proximate analysis and ultimate analysis of raw materials

Description	MSS	Hazelnut shell
Proximate analysis (wt%)		
Moisture[a]	79.54	8.22
Volatile matter[b]	60.34	76.57
Ash[b]	33.43	1.23
Fixed carbon[b]	1.13	13.98
Low heating value (MJ/kg)[b]	14.90	27.82
Ultimate analysis (wt%)[b]		
Carbon content	36.88	48.11
Hydrogen content	4.94	2.62
Nitrogen content	5.03	0.41
Sulfur content	1.14	2.94
Oxygen content[c]	52.01	45.92

[a] Received basis after adding polyacrylamide (0.4 wt%) and dehydration

[b] Dry basis after heating at 105 ± 5 °C for 24 h

[c] Calculated by mass balance

Table 2 The contents of heavy metal in MSS

Element	Heavy metal element content (mg/kg)	Threshold values[a]	
		China pH< 6.5	China pH ≥ 6.5
Cu	117.53	800	1500
Ni	77.27	100	200
Zn	666.67	2000	3000
Pb	110.28	300	1000
Cr	61.38	600	1000
Cd	6.30	5	20

[a] According to Chinese standard methods (GB18918-2002).

Preparation raw materials for co-pyrolysis

MSS and hazelnut shell blend were impregnated by alkaline activating agent K_2CO_3 with different concentration solutions for 24 h. The impregnated weight ratio of raw material and K_2CO_3 solution was 1:1.5. Because of the environment pollution, K_2CO_3 solution was recycled and increased to the target concentration for reuse. After K_2CO_3 activation, the raw material of MSS and hazelnut shell blended with different weight percents was dried at 105 ± 5 °C for 24 h to remove surface water before co-pyrolysis. Co-pyrolysis of sewage sludge and hazelnut shell blend was conducted in a vacuum tube furnace (MTI, OTF-1200-x). Figure 1 shows schematic diagram of pyrolysis apparatus. The blend in a quartz boat was placed in the middle of quartz tube, and the pyrolysis system was presented in the previous work (Xu et al. 2017). Inert atmosphere was achieved by carrier gas (N_2) sweeping (0.3 L/min). The tube furnace was heated to target pyrolysis temperature with heating rate of 10 °C/min for pyrolysis time and then cooling to room temperature. The bio-char was obtained via diluted hydrochloric acid and deionized water washing to remove impurities and then drying and grinding to 1 mm (18 mesh). The bio-chars were transferred to sealed plastic bags for further analysis. The co-pyrolysis conditions of single-factor experiments are named in Table 3.

Physico-chemical properties of the bio-char

The yield of bio-char

The yield of bio-char was calculated from the following equation:

$$\text{Yield of bio-char (wt\%)} = \frac{W_{\text{bio-char}}}{W_{\text{raw materials}}} \times 100\% \quad (1)$$

where $W_{\text{bio-char}}$ and $W_{\text{raw materials}}$ are weight of bio-char and raw materials, respectively. The yield was based on the dry basis weight of raw materials to evaluate the weight loss of thermal decomposition after co-pyrolysis.

The iodine absorption number

The iodine absorption number showed the development of pore structure of the bio-char below 1.0 nm according to the test methods of wooden activated carbon determination of iodine absorption number (GB/T 12496.8-1999). The iodine absorption number also represented the adsorption ability for small molecule impurities below 1.0 nm diameter. The test steps are shown in Table 4. The iodine absorption number was calculated by the following:

$$A = \frac{5 \times 10\,(C_1 - 1.2C_2V_2) \times 127}{M} \times D \quad (2)$$

where A is the iodine number (mg/g), C_1 is the concentration of iodine solution (mol/L), C_2 is the concentration of sodium thiosulfate (mol/L), V_2 is the titration reading (mL), M is adsorbent mass (g), and D is the correction factor.

Surface functional group and crystallographic structure

The functional groups of MSS, hazelnut shell, and the bio-chars were analyzed by FTIR (NICOLET, 380). The pellet was made with 1 wt% of the sample dispersed in KBr. The spectra were investigated in the range of 4000 to 400/cm with a resolution of

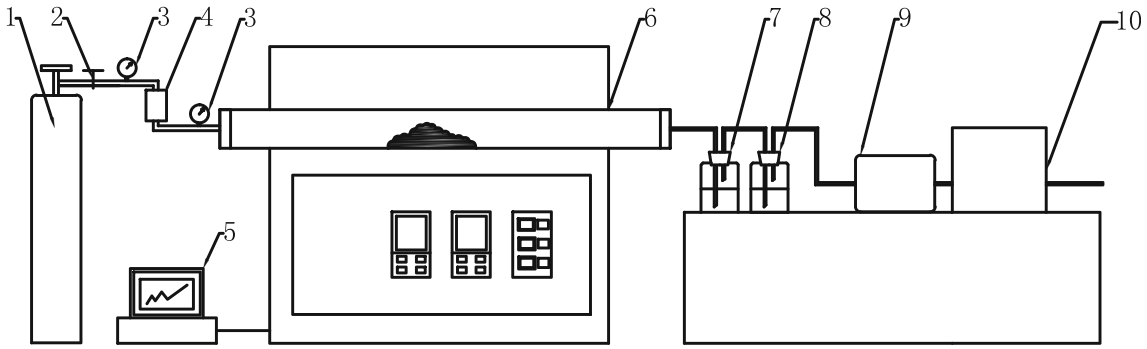

Fig. 1 Experimental apparatus for pyrolysis: 1—inert gas (N_2); 2—valve; 3—pressure gage; 4—flow meter; 5—online temperature monitoring; 6—vacuum tube furnace; 7—acid gas washing bottle; 8—alkaline gas washing bottle; 9—active carbon filter; 10—vacuum pump

Table 3 The named method of produce bio-chars by different process variables

		Type of bio-char			Type of bio-char
Target pyrolysis temperature (°C)	500	T500	Pyrolysis time (min)	30	t30
	600	T600		45	t45
	700	T700		60	t60
	800	T800		75	t75
	900	T900		90	t90
Concentration of activating agent (mol/L)	1	C1	Additive percentage of hazelnut shell (wt%)	5	A5
	1.5	C1.5		10	A10
	2	C2		15	A15
	2.5	C2.5		20	A20
	3	C3		25	A25
	3.5	C3.5		30	A30

4/cm. The baseline of the raw data was adjusted and then the modified data was normalized. XRD (PANalytical B.V., X' Pert PRO) analysis was carried out to identify crystallographic structure of the bio-char sample. The bio-char had been grinded to 200 meshes. The data was collected over a range of 5°–80° using the Cu Kα radiation at a scan rate of 2°/min.

Micromorphology and specific surface areas

The micromorphology was observed by SEM analysis (ZEISS Ultra&Plus, OXFORD X-Max 50 mm^2 (S/N: 52519)). SEM images were recorded to visualize sample morphology, pore structure, and structural changes. The measurements of specific surface areas of the bio-char were made by N_2 adsorption (at 77 K), using a surface analyzer (Micromeritics, ASAP 2020). The bio-char had been pretreated by metal spraying. Specific surface area and N_2 adsorption-desorption isotherm were determined to verify morphology and pore development of the bio-char. Before adsorption/desorption procedure, the bio-char was degassed at 110 °C for 12 h under vacuum to a final pressure of 0.33 Pa. N_2 gas adsorption/desorption isotherms at 77 K were obtained at the relative pressures (P/P_0) that range from 0.01 to 0.99. The specific surface area was calculated according to the method of Langmuir surface area, and average pore volume was calculated according to the Barrett-Joiner-Halenda (BJH) method.

Table 4 The test steps for determination of iodine absorption number

Test step	Operation
1	About 0.2–0.5 g of bio-char was mixed with 10 mL of HCl (V 1 + 9) and lowly heated for about 30 s
2	The samples were cool down to room temperature. Then, the samples were shaken with 50 mL of 0.1 mol/L iodine solution for 15 min
3	The dilute filtrate was titrated with 0.1 mol/L sodium thiosulfate until the solution turned pale yellow
4	2 mL of 1% starch indicator solution was added and titrated until the solution was colorless

BCR sequential extraction experiment

The heavy metals in MSS and bio-chars were sequentially extracted by the modified version of BCR-three step sequential extraction procedure aimed to test the long-term stability of material. The applicability of an improved version of the BCR three-step sequential extraction procedure on the sewage sludge was used (Rauret et al. 2000). It has been widely applied in quantifying chemical speciation distribution of heavy metals in sludge, soil, and sediment. The contents of heavy metals were measured by ICP instrument. The fractions of heavy metals can be divided into four categories: acid soluble/exchangeable (F1), reducible (F2), oxidizable (F3), and residual (F4) fractions through BCR sequential extraction. The concentrations of heavy metals in acid soluble/exchangeable, reducible, and oxidizable fractions can be determined directly by ICP instrument. The residual fraction of bio-char samples were digested in 20 mL aqua regia with microwave assistance according to the method of Katherine and Christine (2003) before detection by ICP.

Adsorption experiments

Adsorption experiments were conducted to determine adsorption capacity, equilibrium model, and kinetic model of the bio-char for Cu(II) adsorption. The bio-char had been grinded to 200 meshes. Cu(II) solutions used in adsorption capacity and adsorption isothermal model experiments were prepared by deionized water and $CuSO_4{\cdot}5H_2O$, and $C_0 = 0$, 20, 40, 50, 60, 75, 80, and 100 mg/L. The bio-char dosage was 1.25 g/L, and Erlenmeyer flasks were sealed and shaken at a constant speed of 110 rpm at 25 °C for 24 h. For kinetic model

experiment, the initial concentration of Cu(II) was 55 mg/L. The bio-char dosage was 1.25 g/L, and Erlenmeyer flasks were sealed and shaken at a constant speed of 110 rpm at 25 °C for 0 min, 10 min, 30 min, 1 h, 2 h, 5 h, 10 h, and 24 h. After the solid-liquid separation by a filter membrane (0.45 μm) at the end of adsorption, Cu(II) concentration was measured by ICP instrument. The adsorption capacity of the bio-char was calculated according to Eq. (3),

$$Q_e = \frac{(C_0 - C_e)V}{M} \tag{3}$$

where Q_e (mg/g) is adsorption quantity; C_0 (mg/L) and C_e (mg/L) are initial and equilibrium concentration, respectively; V (L) is volume of solution; and M (g) is mass of the bio-char.

Results and discussion

The yield and the iodine absorption number of bio-chars by different process variables

The yield and the iodine absorption number of the bio-chars under different process variables, such as final pyrolysis temperature, pyrolysis time, concentration of activation reagent K_2CO_3, and additive percentage of hazelnut shell, are shown in Fig. 2. The yield of the bio-chars decreased with increasing of the final pyrolysis temperature, as shown in Fig. 2a, from 61.00 to 34.87% after increasing temperature from 500 to 900 °C. This result is similar to previous studies (Agrafioti et al. 2013), in which the increase in pyrolysis temperature resulted in a significant decrease in bio-char yield. Due to gradual decomposition of organic and non-organic substances in raw materials, the yield of bio-char also decreased from 43.95 to 36.78% with increasing of pyrolysis time. The mass loss is derived from the content volatile matter of raw materials. Pyrolysis temperature increasing and time extension cause further decomposition of organic and non-organic substances. In a similar way, increasing additive percentage of hazelnut shell will cause decrease of the yield because of the higher volatile matter of hazelnut shell than MSS. Thus, 30 wt% hazelnut shell contributes to both yield and control of heavy metal contents. However, the concentration of activation reagent K_2CO_3 does not significantly influence on yield, only 2.32% mass loss from 1 to 4 mol/L shown in Fig. 2c.

The iodine absorption number is used to determine microporous characteristic and micromolecule adsorption capacity of bio-char. High iodine absorption number means that the bio-char has abundant microporous constructions and further adsorption application prospect. Four kinds of process variables all have significant influences on the iodine absorption number, as shown in Fig. 2. Simply increasing final pyrolysis temperature or pyrolysis time cannot bring higher iodine absorption number. Appropriate process variables can contribute the yield and the iodine absorption number of bio-char and prevent to etch pore structure excessively to collapse. The bio-char derived by 850 °C and 45 min had the iodine absorption number of 1068.22 mg/g, which is higher than that of the other condition of process variables. Increasing additive percentage of hazelnut shell can also contribute to micromolecule adsorption capacity, and iodine absorption number increased 362.09 mg/g from 0 to 30%. Varying the concentration of activation reagent K_2CO_3 from 1 to 4 mol/L, the iodine absorption number showed an uptrend from 270.75 to 812.41 mg/g, which means that K_2CO_3 significantly improves adsorption capacity. In the case of K_2CO_3 activation, during the carbonization, the K_2CO_3 was decomposed in the inert atmosphere by the edge carbons to form atomic K and CO, and the reaction of that is shown in Eq. (4) (Hunsom and Autthanit 2013)

$$K_2CO_3 + 2C \rightarrow 2K + 3CO \tag{4}$$

The activation mechanism of K_2CO_3 is expounded that K_2CO_3 molecules reacts with C to etch raw materials and decomposes CO to develop pore structure when heated in tubular furnace. However, higher temperature and longer pyrolysis time might widen the micropore to mesopore or macropore because of the further etching effect, which will not increase but decrease the iodine absorption number, even the specific surface area of bio-chars.

FTIR spectra and XRD of bio-chars

FTIR spectrometry is used to qualitatively determine the changes of surface functional groups and deduce chemical reactions. The bio-char samples were made by raw materials (the weight of hazelnut shell is 30% and concentration of activating agent is 4 mol/L) at different final pyrolysis temperatures with $\beta = 10$ °C/min and hold the target temperature for 60 min during co-pyrolysis. The FTIR spectra demonstrated that the functional characteristics of bio-chars are similar, but different from the raw materials, especially hazelnut shell (Fig. 3). Compared with MSS, hazelnut shell had some peaks from 1513 to 1263/cm, indicating that hazelnut shell has more functional groups than MSS.

Pyrolysis led to important changes in the organic matter of raw materials. The peaks at 3423/cm showed O-H structure of all samples, and O-H structure was derived from carbohydrate, alcohol, and molecular water in bio-char and raw material samples. For raw materials, the peak at 2923 and 2858/cm represented alkane C-H symmetrical stretching vibrations and antisymmetric stretching vibrations. The stretching vibrations disappeared from raw

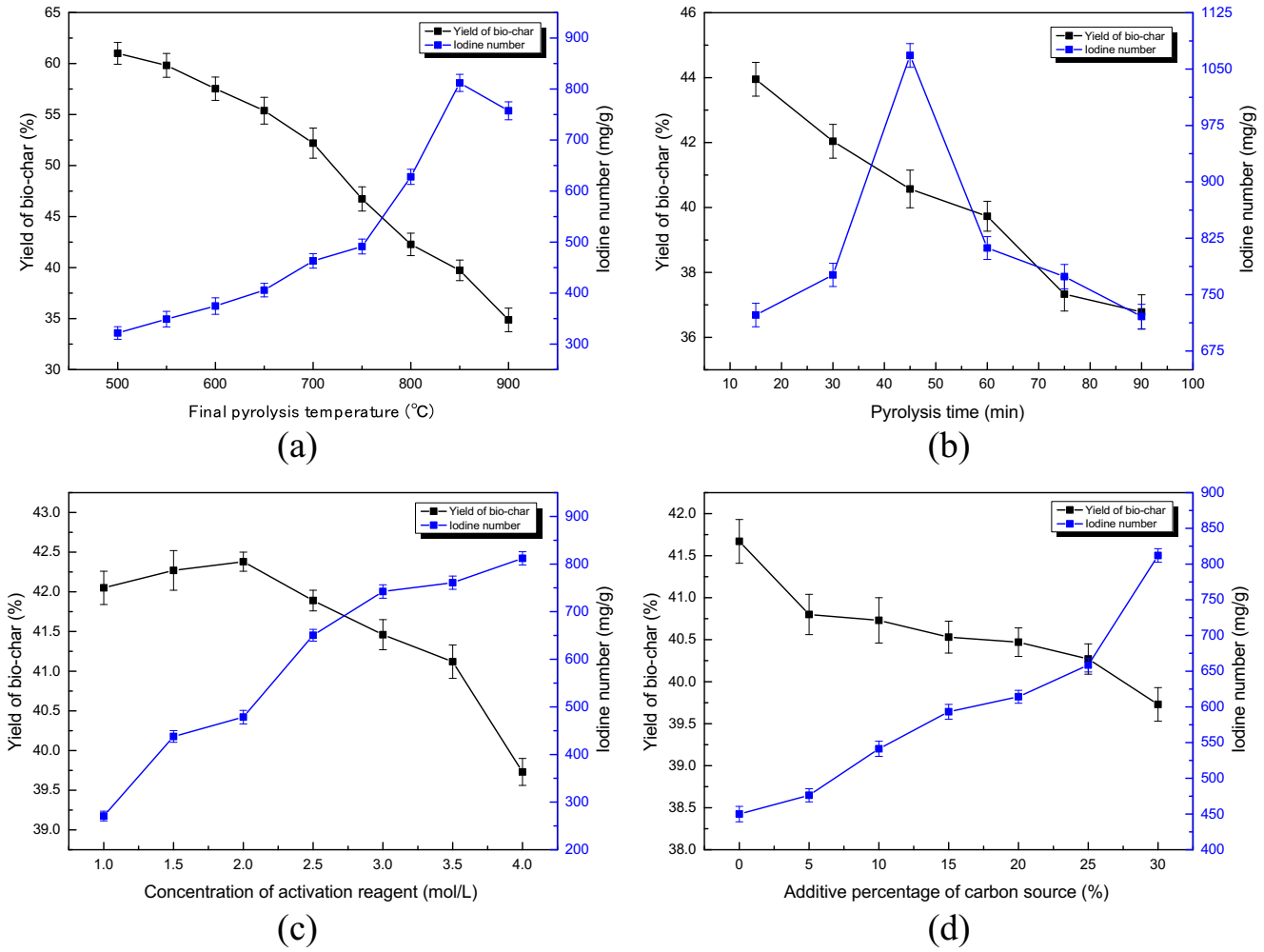

Fig. 2 The yield and the iodine absorption number of the bio-chars under different process variables. **a** Tt60C4A30. **b** T850tC4A30. **c** T850t60CA30. **d** T850t60C5A

materials to bio-char after pyrolysis at 700 °C, which means that with temperature increasing, hydrocarbon is decomposed to short chain and released gradually. For the bio-char samples under different temperatures, the peak at 1643/cm appeared with pyrolysis temperature increasing, which represents C=O stretching vibrations from ketone, aldehyde, lactone, and carboxyl. The double peaks at 1479 and 1413/cm appeared in bio-char samples and represented CO_3^{2-} symmetrical stretching vibrations because of addition of activating agent K_2CO_3. And the peaks at 688/cm that appeared in bio-char samples also mean CO_3^{2-} in-plane bending vibration. During pyrolysis, various forms of oxygen in raw materials banded with carbon element and the C-O stretching vibrations at 1035/cm represented aromatic esters, aliphatic ester, and fat fractions. The fingerprint spectra below 1000/cm were quite identical in bio-char samples due to the mineral content pyrolyzed. These oxygenated functional groups were normally related to the acidity of samples (Martin et al. 2003).

The crystal structure of MSS and the bio-char co-pyrolyzed at 800 °C with alkaline activating agent K_2CO_3 was measured by XRD and is presented in Fig. 4. As shown in Fig. 4a, MSS had inorganic elements of Ca, Al, Fe, Si, and O. Before pyrolysis, the simple inorganic ingredients were constituted by inorganic elements and the major crystal structures were from SiO_2, $CaSO_4$, Fe_2O_3, and $Ca(Al_2Si_2O_8)$. However, after pyrolysis, the obvious diffraction peaks appeared at $2\theta = 24°$and 43° as shown in Fig. 4b. These two peaks that appeared at (002) and (100) are typical characteristic peaks of carbon (Baek et al. 2016). After co-pyrolysis at 800 °C, the diffraction peaks became strong and broad and appeared amorphous structure. Because of high pyrolysis temperature, raw materials were decomposed substantially, and the bio-char was transformed into graphitization. Song et al. (2017) found similar diffraction peaks, and it was derived that the carbon gradually transformed into graphite under high temperature. Combined with the surface area results in the

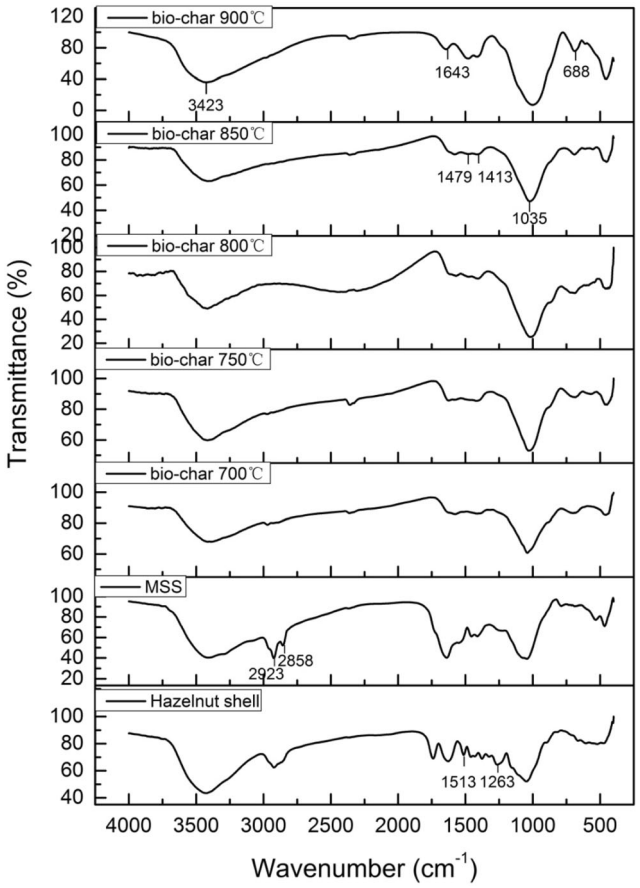

Fig. 3 FTIR of MSS, hazelnut shell, and bio-chars produced at different temperatures

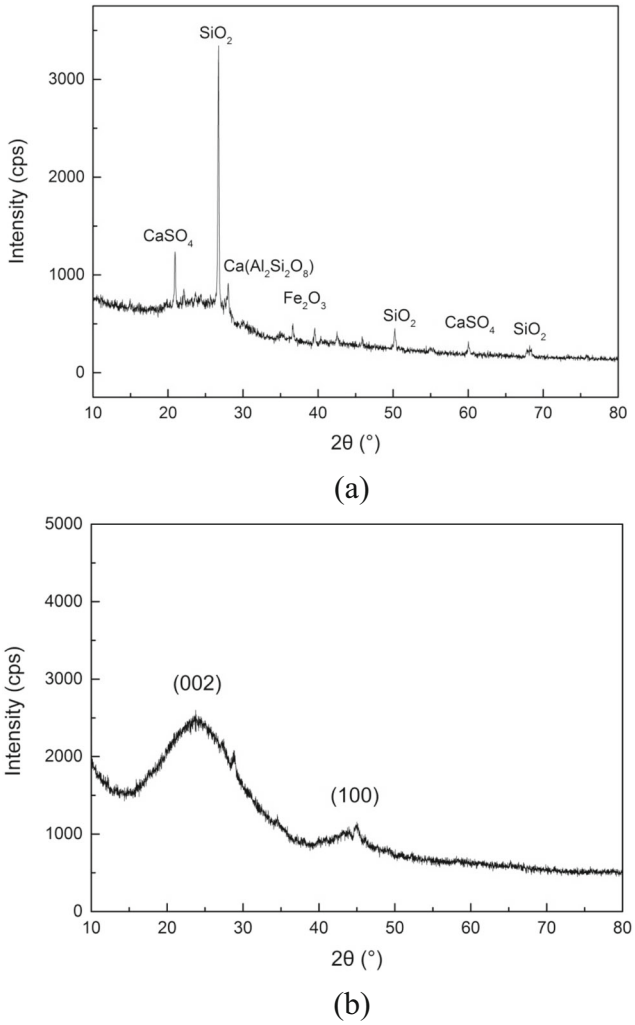

Fig. 4 XRD of MSS (**a**) and the bio-char (**b**) (30 wt% hazelnut shell and 70 wt% MSS) with $\beta = 10$ °C/min to 800 °C for 60 min

"Micromorphology and specific surface areas of bio-chars" section, the formation of amorphous structure was from excessive thermal decomposition of raw material under high temperature, which made carbon skeleton graphitization. However, the amorphous structure was conductive to the formation of micropore and pore volume contributing to adsorption application.

Micromorphology and specific surface areas of bio-chars

SEM images present visual understanding of micromorphology. SEM images of MSS and different bio-chars are shown in Fig. 5 at the optimum operating condition with × 5000–10,000 magnifications. There was no pore structure in raw MSS (Fig. 5a). As shown in Fig. 5b, there were insufficient micropores and mesoporous, but nucleation and crystallization in the bio-char without chemical activation.

After chemical activation of K_2CO_3, the bio-char shown in Fig. 5c, d had abundant pore structure, which is from micropores (< 2 nm) and mesoporous (2–50 nm) mainly. During co-pyrolysis, activating agent K_2CO_3 released gaseous molecule and reacted with C to etch pore. These two reasons contributed to produce and extend pore structure for the bio-char together. The homogeneous dispersibility provided by hazelnut shell made pore structure that grows uniformly and produced a uniform microstructure. After washing by dilute hydrochloric acid solution and deionized water to remove pyrolysis impurities, pore structure became clear, and the micropores and mesoporous brought remarkable specific surface area. Combined with the iodine absorption number of bio-chars, SEM images confirmed that the further chemical activation will extend pore structure to collapse with increasing of pyrolysis temperature and time. The collapse of pore structure will influence surface area of bio-char. Langmuir surface area also confirms this viewpoint in Table 5. The surface area of the bio-char reached 1990.23 m^2/g after 850 °C with activating agent K_2CO_3. The variation trend is in accordance with the iodine absorption number of bio-

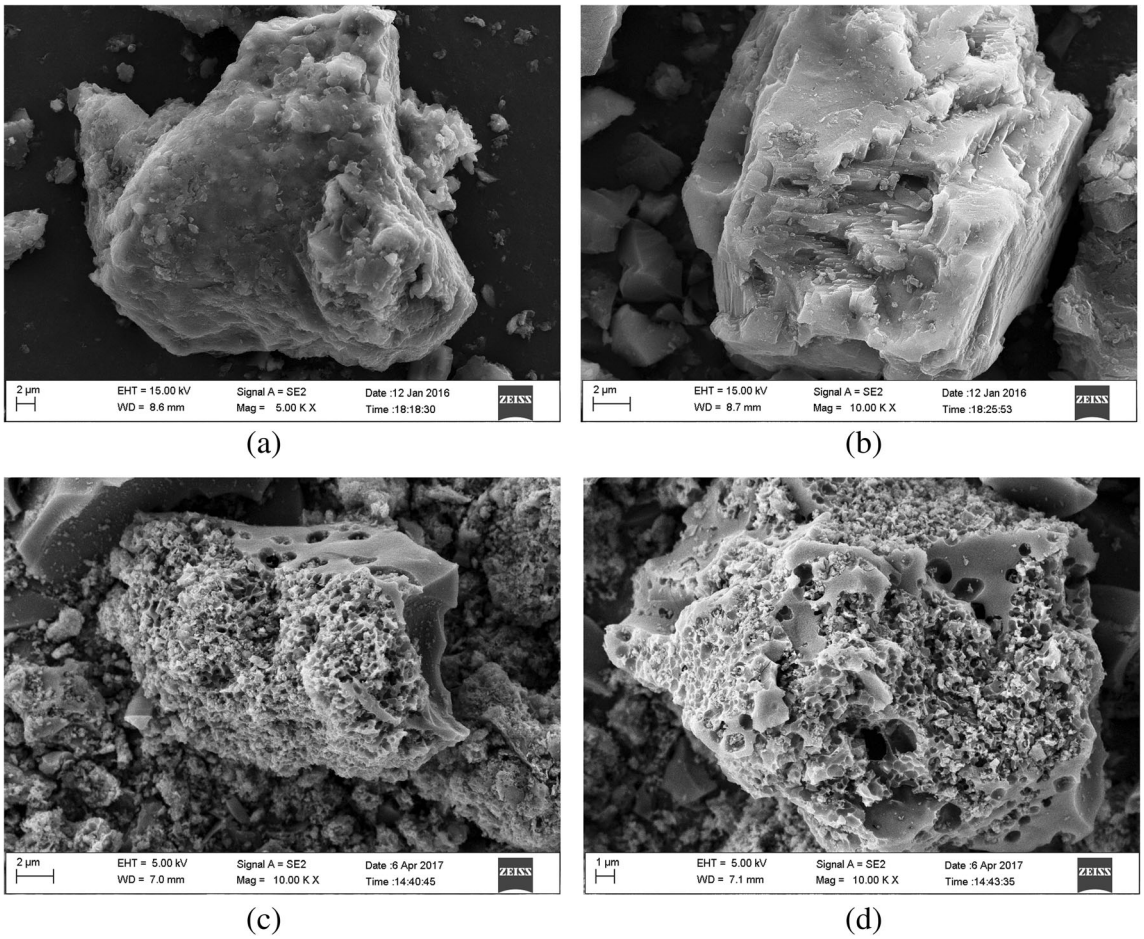

Fig. 5 SEM micrographs of MSS (**a**), the bio-char from MSS after pyrolysis for 500 °C and 90 min without chemical activation (**b**), and the bio-char from MSS and hazelnut shell blend after co-pyrolysis for 850 °C and 45 min with 4 mol/L activating agent K_2CO_3 (**c**, **d**)

char under co-pyrolysis temperature condition in the "The yield and the iodine absorption number of bio-chars by different process variables" section. For pore structure of bio-chars, pore diameter was close to micropore, and proportionable micropore volume can be used for further adsorption application. The data on surface area and pore volume of bio-chars is in agreement with previous studies using similar feedstocks (Yuan et al. 2013), which confirms that MSS can be transformed to valuable carbon material and applied to the adsorption of pollutant.

BCR sequential extraction experiment of heavy metals

The chemical speciation of heavy metals decides the bioavailability and toxicity in the environment (Huang and Yuan 2016), and the modified BCR sequential extraction is used to assess the chemical speciation of heavy metals. The heavy metals can be categorized into four fractions by BCR sequential extraction. From F1 to F4, the degree of immobilization of heavy metals increases gradually, and the bio-

Table 5 Microstructure properties of bio-chars under different pyrolysis temperatures

Sample	Langmuir surface area(m^2/g)	Micropore volume(cc/g)	Pore diameter(nm)
BC-T500	874.61	0.442	4.10
BC-T600	1285.47	0.458	3.89
BC-T700	1612.24	0.426	3.58
BC-T800	1784.45	0.414	3.57
BC-T850	1990.23	0.589	3.05
BC-T900	1456.63	0.435	3.94

availability and toxicity can be decreased (Chen et al. 2015). Heavy metals distributed in F1 and F2 are easily available uptake by plants and animals to enter the biological chain, and so it is identified as directly toxic and bio-available fractions. The F3 fraction, as the potentially bio-available fraction, can be degraded and leached under very rigorous conditions (highly acidic conditions and oxidizing atmosphere). The F4 fraction is recognized as non-toxic and non-bio-available, because the heavy metals are immobilized in the crystalline structures (Jin et al. 2017).

The raw material and bio-chars of co-pyrolysis by 70% MSS and 30% hazelnut shell were obtained at different final pyrolysis temperatures. The species distribution of heavy metals obtained by BCR sequential extraction is presented in Fig. 6. For the raw material, the concentration of Cu was 38.59% in F3 fraction, which may be attributed to the high stability of Cu-organic matter complexes in MSS (Shi et al. 2013). Cr and Zn were mainly present in the F2 fraction (39.44 and 63.61%, respectively), and Cu, Ni, Cd, and Pb had higher concentrations in the F4 fraction (44.83, 42.93, 41.88, and 74.33%, respectively). Final pyrolysis temperature is the crucial factor of migration and stabilization of heavy metals. Compared with the previous work of our team (Zhao et al. 2017), higher temperature changes the heavy metal distribution of chemical speciation, and from 600ºC to 1000ºC, the degree of immobilization increased observably. After co-pyrolysis at 600 °C, the F3 fraction of Cu was 9.13% and the F4 fraction of Cu was 90.83% of the bio-char. The sum of F3 and F4 fraction of Cu exceeded 94.90% above 600 °C. Yuan et al. (2011) indicated that Cu is associated with strong organic ligand and probably contained in minerals like feldspars and quartz with less mobility and potential bio-availability. Ni had an excellent behavior of immobilization. After co-pyrolysis at 600 °C, the F4 fraction of the bio-char increased 52.13% compared with the raw material and retained above 89.43% from 600 to 1000 °C. For Ni, the fractions of F1 and F2 were 0.87 and 0.86% respectively at 1000 °C. After pyrolysis, Cr presented residual fraction from 87.51 to 97.33% with temperature increasing from 600 to 1000 °C, which also achieves outstanding immobilization behavior. However, the F4 fractions of Cd decreased 5.47% from 600 to 1000 °C. Because of lower boiling point of Cd (765 °C), it is concluded that during the co-pyrolysis process of decomposition and conversion of the raw material, the F3 and F4 fractions of Cd transfer to gas production, which has the same conclusion with other researcher (Shao et al. 2015). Specifically, Pb and Zn had similar immobilization behavior, the fraction of F1 and F2 can be negligible nearly above 800 °C, and the fraction of F4 exceeded 95% already. For Zn, the fraction of F1 and F2 decreased by 0.60 and 4.51% from 600 to 1000 °C. And after 1000 °C co-pyrolysis, the fractions of F1 and F2 can be ignored nearly. For Pb, the bio-char had just 0.42% of F1 fraction and 1.42% of F2 fraction after 1000 °C. The residual fractions of heavy metals were above 92.95% after co-pyrolysis at 900 °C except Cd, and the bio-char presented significant immobilization behavior.

In summary, heavy metals have different behaviors in immobilization process. The heavy metals of the directly toxic and bio-available fraction (F1 + F2) in the raw material decreased significantly after co-pyrolysis above 600 °C. Addition of hazelnut shell leads to decrease of the content heavy metals, and high temperature further transforms the bio-char to a more stable form. Co-pyrolysis has positive effects on immobilization of heavy metals in the raw material, and final pyrolysis temperature has significant influence on the stabilization in the bio-chars, which helps bio-chars to decrease the toxicity of heavy metals for further application.

Isothermal adsorption model and kinetic model of Cu(II) by the bio-char

The different initial concentrations of Cu(II) ranging from 20 to 100 mg/L were used to analyze adsorption capacity of the bio-char. The bio-char was produced by co-pyrolysis with 30% hazelnut shell at 850 °C for 45 min after 4 mol/L K_2CO_3 activation, which has the surface area of 1990.23 m^2/g. After 24 h adsorption process, Cu(II) equilibrium concentration in solution is shown in Fig. 7a, and the N_2 adsorption-desorption isotherm of the bio-char is shown in Fig. 7b. As shown in Fig. 7a, the maximum adsorption capacity of bio-char for Cu(II) was 42.28 mg/g after 24 h when initial concentration was 100 mg/L. According to IUPAC classification (Sing et al. 1985), the N_2 adsorption-desorption isotherm of the bio-char was similar to type IV isotherm and type H2 hysteresis loop. The behavior indicates that the pores of the bio-char are mainly mesopores, which is also verified by SEM images in Fig. 5, and has bigger volume of pore structure. The capillary condensation would occur in the pores, and the pores had narrow necks and wide bodies, often referred to as ink bottle pores.

To express maximum adsorption capacities of Cu(II) and adsorption mechanism, the adsorption isotherms were analyzed by two established fundamental models, Langmuir model and Freundlich model. The Langmuir isotherm model is used to describe the monolayer adsorption process, and all sites on specific surface participate in adsorption (Xue et al. 2013). The Freundlich isotherm model assumes that adsorption process occurs on specific surface through multilayer adsorption (Wang et al. 2017). The equations are given as follows:

$$\text{Langmuir isotherm}: \frac{C_e}{Q_e} = \frac{1}{k_L Q_m} + \frac{C_e}{Q_m} \quad (5)$$

where C_e (mg/L) is equilibrium concentration of adsorbate, Q_e (mg/g) is adsorption quantity of equilibrium, Q_m (mg/g) is

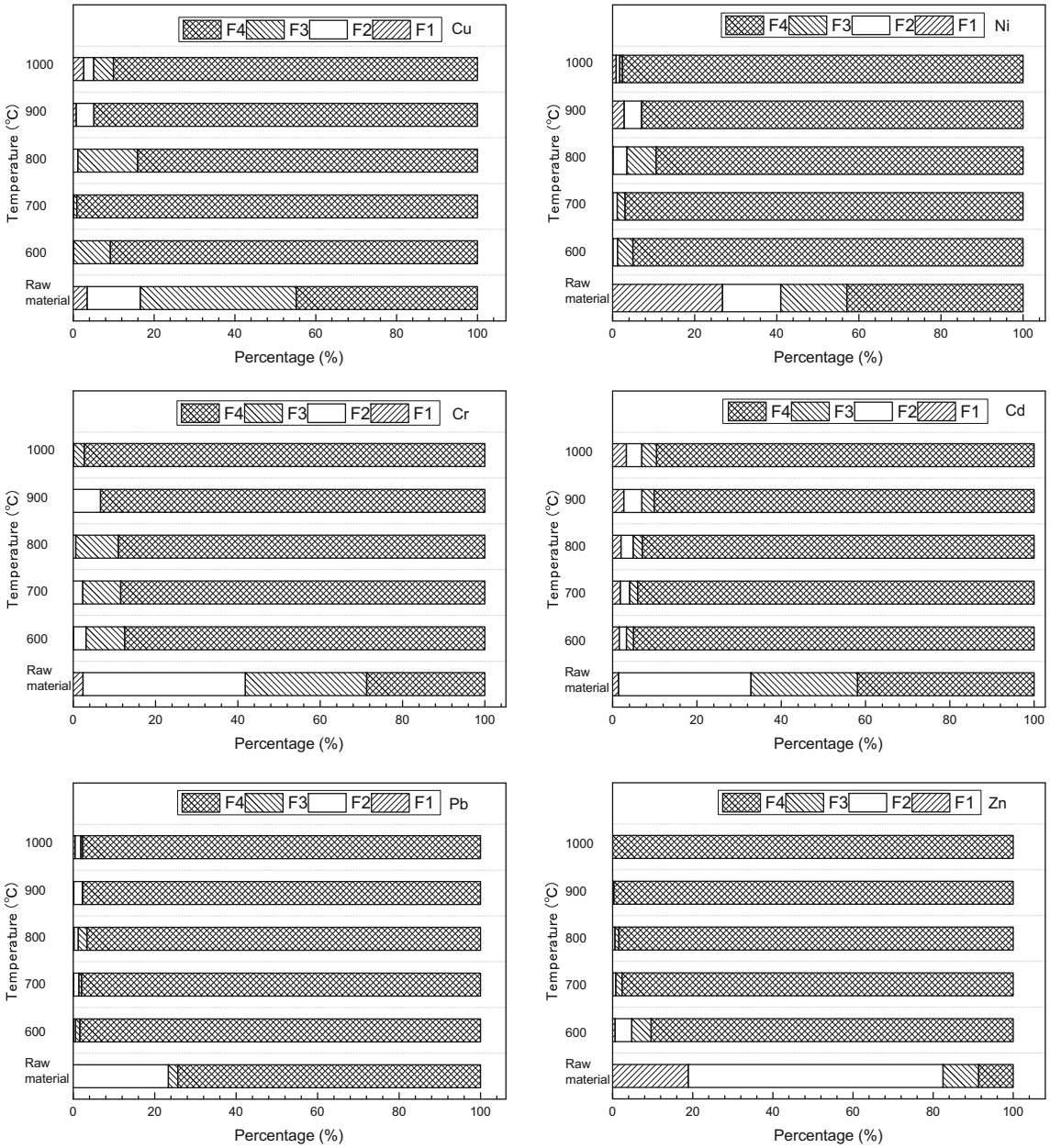

Fig. 6 The BCR sequential extraction of the raw material and bio-chars about Cu, Ni, Cr, Cd, Pb, and Zn

theoretical maximum monolayer adsorption capacity of adsorbate, and k_L (L/mg) is the Langmuir isotherm coefficients.

$$\text{Freundlich isotherm}: \ln Q_e = \ln k_F + \frac{\ln C_e}{n} \quad (6)$$

where k_F (L/mg) is the Freundlich isotherm coefficients, and n is the adsorption constants of Freundlich.

The fitting parameters of Cu(II) adsorption process by the bio-char are listed in Table 6. The linear correlation coefficient R^2 indicated that the Langmuir model was fitting well to the isotherm data with higher R^2 value comparing to Freundlich model, due to homogeneous distribution of active sites on the bio-char surface. The Cu(II) theoretical maximum monolayer adsorption capacity of the bio-char was 43.54 mg/g, which was a little more than the Q_e after 24 h adsorption process. A good fit with the Langmuir model is in good agreement with the studies of other author (Bogusz et al. 2017). The results of Langmuir model demonstrate that homogeneous monolayer Cu(II) is covered on the surface of bio-char particles. Furthermore, the adsorption of Cu(II) was a dynamic chemisorption process by the adsorption affinity of physiochemical heterogeneity from surface functional groups of the bio-char. The values of n in Table 6, between 1 and 10,

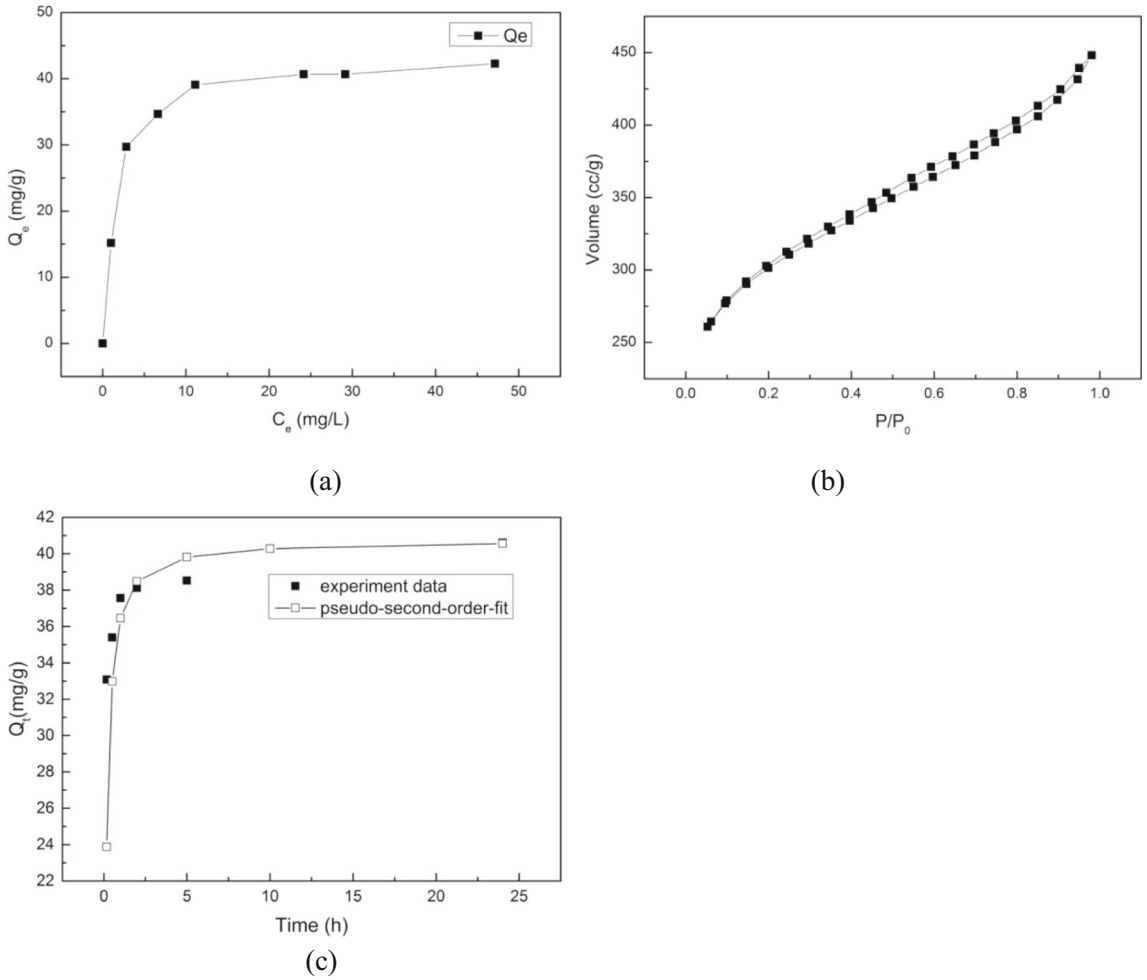

Fig. 7 Cu(II) equilibrium concentration (**a**), N_2 adsorption-desorption isotherms (**b**), and fitting of kinetic model (**c**) of the bio-char

indicate heterogeneity of the adsorbents (Zhang et al. 2005). Although, the adsorption capacity of the bio-char derived from MSS and hazelnut shell is not the highest one, it can be obtained cheaply in large quantities and safety.

The adsorption kinetics is investigated to detect the adsorption progress and the control factor of chemical or physical mechanism (Cao et al. 2014). The kinetic models of pseudo-first-order model and pseudo-second-order model are used to determine the relationship between the amount of adsorbate and reaction time. The two equations were expressed as follows:

$$\text{Pseudo-first-order model}: \lg(Q_e - Q_t) = \lg Q_e - \frac{k_1}{2.303}t \quad (7)$$

$$\text{Pseudo-second-order model}: \frac{t}{Q_t} = \frac{1}{k_2 Q_e^{\,2}} + \frac{t}{Q_e} \quad (8)$$

Table 6 The fitting parameters of equilibrium model and kinetic model

Langmuir isotherm model		Freundlich isotherm model	
Q_m (mg/g)	43.54	k_F (L/mg)	19.29
k_L (L/mg)	0.62	n	4.19
R^2	0.99963	R^2	0.77546
Pseudo-first-order model		Pseudo-second-order model	
Q_e (mg/g)	5.72	Q_e (mg/g)	40.75
k_1 (/h)	0.28	k_2 (mg/g h)	0.21
R^2	0.90442	R^2	0.99989

where Q_e (mg/g) is adsorption quantity of equilibrium; Q_t (mg/g) is the adsorption quantity of time t (h); and k_1 (1/h) and k_2 (mg/g h) are the equilibrium rate constant of pseudo-first-order adsorption and pseudo-second-order adsorption, respectively.

As shown in Fig. 7c, variation tendency of adsorption quantity over 24 h was flat gradually, and the adsorption quantity of 24 h achieved 40.60 mg/g. After adsorption process of 1 h, the adsorption quantity increased to 37.56 mg/g. The adsorption of Cu(II) during initial time is rapid because of the abundant vacant active sites until these activated site are further saturated. These results are similar to those of bio-char derived from other agricultural residue (Pellera et al. 2012). The values of k_1, k_2, Q_e, and R^2 of kinetic model are shown in Table 6, and the linear correlation coefficient R^2 of pseudo-second-order model was higher, which suggests that it can be applied for the entire adsorption process. The adsorption quantity of equilibrium of pseudo-second-order adsorption was 40.75 mg/g, which is approximate to the adsorption quantity of 24 h and the theoretical maximum monolayer adsorption capacity of Langmuir isotherm model, just a small interval between Q_e(exp) and Q_e(cal). As the result of Langmuir isotherm model shown, it is also confirmed that the chemisorption is the rate-limiting mechanism for the adsorption of Cu(II) of the bio-char. Similar results were reported in Cu(II) adsorption by the bio-chars produced from *Spartina alterniflora* (Li et al. 2013). For bio-char adsorbents, the structural properties such as micromorphology, surface areas, pore type, and pore volume could affect the adsorption performance synthetically. And surface functional groups also act as active binding sites for adsorption. A possible mechanism of adsorption of Cu(II) is complex. The adsorption mechanism of binding with surface functional groups containing oxygen belongs to surface chemistry adsorption, which is in accordance with Langmuir model. Determining the predominant mechanism depends on the type of bio-char. In the "FTIR spectra and XRD of bio-chars" section, the presence of O-H, C-O, and C=O stretching vibrations had been confirmed on the surface of bio-chars, which is from complex biomass material pyrolysis. Therefore, it is deduced that Cu(II) is adsorbed on surface of the bio-char particle via chemical interaction and surface functional groups bond, which requires a long time to achieve equilibrium.

Conclusion

Higher temperature and longer time decreased the iodine absorption number of bio-chars because of the further etching effect. Pyrolysis temperature led to important changes of function groups and the bio-char transformed into graphitization above 800 °C. The surface area of bio-char reached 1990.23 m^2/g after 850 °C by abundant micropore and mesoporous structure. Co-pyrolysis promoted heavy metal transformation from mobile fraction to stable fraction and presented significant immobilization behavior above 900 °C. Surface functional groups acted as active binding sites for Cu(II) adsorption, and the process can be described by Langmuir model and pseudo-second-order model.

Funding information This research work was supported by the National Water Pollution Control and Management Technology Major Projects (2014ZX07201-009-04), the Liaoning Province Natural Science Foundation (2014020036), and the Fundamental Research Funds for the Central Universities (N160106005).

References

Agrafioti E, Bouras G, Kalderis D, Diamadopoulos E (2013) Biochar production by sewage sludge pyrolysis. J Anal Appl Pyrol 101: 72–78

Baek J, Lee HM, Roh JS, Lee HS, Kang HS, Kim BJ (2016) Studies on preparation and applications of polymeric precursor-based activated hard carbons: I. Activation mechanism and microstructure analyses. Micropor Mesopor Mat 219:258–264

Bakisgan C, Dumanli AG, Yürüm Y (2009) Trace elements in Turkish biomass fuels: ashes of wheat straw, olive bagasse and hazelnut shell. Fuel 88(10):1842–1851

Bogusz A, Nowak K, Stefaniuk M, Dobrowolski R, Oleszczuk P (2017) Synthesis of biochar from residues after biogas production with respect to cadmium and nickel removal from wastewater. J Environ Manag 201:268–276

Bondarczuk K, Markowicz A, Piotrowska-Seget Z (2016) The urgent need for risk assessment on the antibiotic resistance spread via sewage sludge land application. Environ Int 87:49–55

Cao YC, Pawłowski A (2012) Sewage sludge-to-energy approaches based on anaerobic digestion and pyrolysis: brief overview and energy efficiency assessment. Renew Sust Energ Rev 16(3):1657–1665

Cao JS, Lin JX, Fang F, Zhang MT, Hu ZR (2014) A new absorbent by modifying walnut shell for the removal of anionic dye: kinetic and thermodynamic studies. Bioresour Technol 163:199–205

Chen D, Yin L, Wang H, He P (2014) Pyrolysis technologies for municipal solid waste: a review. Waste Manag 34(12):2466–2486

Chen FF, Hu YY, Dou XM, Chen DZ, Dai XH (2015) Chemical forms of heavy metals in pyrolytic char of heavy metal-implanted sewage sludge and their impacts on leaching behaviors. J Anal Appl Pyrolysis 116:152–160

Fang W, Wei YH, Liu JG (2016) Comparative characterization of sewage sludge compost and soil: heavy metal leaching characteristics. J Hazard Mater 310:1–10

Fernando NL, Fedorak PM (2005) Changes at an activated sludge sewage treatment plant alter the numbers of airborne aerobic microorganisms. Water Res 39:4597–4608

Fytili D, Zabaniotou A (2008) Utilization of sewage sludge in EU application of old and new methods—a review. Renew Sust Energ Rev 12(1):116–140

Hoşgün EZ, Berikten D, Kıvanç M, Bozan B (2017) Ethanol production from hazelnut shells through enzymatic saccharification and fermentation by low-temperature alkali pretreatment. Fuel 196:280–287

Huang HJ, Yuan XZ (2016) The migration and transformation behaviors of heavy metals during the hydrothermal treatment of sewage sludge. Bioresour Technol 200:991–998

Hunsom M, Autthanit C (2013) Adsorptive purification of crude glycerol by sewage sludge-derived activated carbon prepared by chemical activation with H_3PO_4,? K_2CO_3? and KOH. Chem Eng J 229: 334–343

Jin JW, Li YN, Zhang JY, Wu SC, Cao YC, Liang P, Zhang J, Wong MH, Wang MY, Shan SD, Christie P (2016) Influence of pyrolysis temperature on properties and environmental safety of heavy metals in biochars derived from municipal sewage sludge. J Hazard Mater 320:417–426

Jin JW, Wang MY, Cao YC, Wu SC, Liang P, Li YN, Zhang JY, Zhang J, Wong MH, Shan SD, Christie P (2017) Cumulative effects of bamboo sawdust addition on pyrolysis of sewage sludge: biochar properties and environmental risk from metals. Bioresour Technol 228: 218–226

Katherine FM, Christine MD (2003) Comparison of original and modified BCR sequential extraction procedures for the fractionation of copper, iron, lead, manganese and zinc in soils and sediments. Anal Chim Acta 478(1):111–118

Li M, Liu Q, Guo LJ, Zhang YP, Lou ZJ, Wang Y, Qian GR (2013) Cu(II) removal from aqueous solution by Spartina alterniflora derived biochar. Bioresour Technol 141:83–88

Martin MJ, Artola A, Balaguer MD, Rigola M (2003) Activated carbons developed from surplus sewage sludge for the removal of dyes from dilute aqueous solutions. Chem Eng J 94(3):231–239

Okman I, Karagöz S, Tay T, Erdem M (2014) Activated carbons from grape seeds by chemical activation with potassium carbonate and potassium hydroxide. Appl Surf Sci 293:138–142

Pellera FM, Giannis A, Kalderis D, Anastasiadou K, Stegmann R, Wang JY, Gidarakos E (2012) Adsorption of Cu(II) ions from aqueous solutions on biochars prepared from agricultural by-products. J Environ Manag 96(1):35–42

Rauret G, López-Sánchez JF, Sahuquillo A, Barahona E, Lachica M, Ure AM, Davidson CM, Gomez A, Lück D, Bacon J, Yli-Halla M, Muntau H, Quevauviller P (2000) Application of a modified BCR sequential extraction (three-step)procedure for the determination of extractable trace metal contents in a sewage sludge amended soil reference material (CRM 483),complemented by a three-year stability study of acetic acid and EDTA extractable metal content. J Environ Monitor 2(3):228–233

Shao JG, Yuan XZ, Leng LJ, Huang HJ, Jiang LB, Wang H, Chen XH, Zeng GM (2015) The comparison of the migration and transformation behavior of heavy metals during pyrolysis and liquefaction of municipal sewage sludge, paper mill sludge, and slaughterhouse sludge. Bioresour Technol 198:16–22

Shi W, Liu C, Ding D, Lei Z, Yang Y, Feng C, Zhang Z (2013) Immobilization of heavy metals in sewage sludge by using subcritical water technology. Bioresour Technol 137:18–24

Sing KSW, Everett DH, Haul RAW, Moscou L, Pierotti RA, Rouquerol J, Siemieniewska T (1985) Reporting physisorption data for gas solid systems with special reference to the determination of surface-area and porosity. Pure Appl Chem 57(4):603–619

Song X, Li K, Ning P, Wang C, Sun X, Tang LH, Ruan HT, Han S (2017) Surface characterization studies of walnut-shell biochar catalysts for simultaneously removing of organic sulfur from yellow phosphorus tail gas. Appl Surf Sci 425:130–140

Tran HN, You SJ, Chao HP (2017) Fast and efficient adsorption of methylene green 5 on activated carbon prepared from new chemical activation method. J Environ Manag 188:322–336

Wang P, Tang L, Wei X, Zeng GM, Zhou YY, Deng YC, Wang JJ, Xie ZH, Fang W (2017) Synthesis and application of iron and zinc doped biochar for removal of p-nitrophenol in wastewater and assessment of the influence of co-existed Pb(II). Appl Surf Sci 392: 391–401

Wei LL, Zhao QL, Hu K, Lee DJ, Xie CM, Jiang JQ (2011) Extracellular biological organic matters in sewage sludge during mesophilic digestion at reduced hydraulic retention time. Water Res 45:1472–1480

Xu XY, Zhao B, Sun ML, Chen X, Zhang MC, Li HB, Xu SC (2017) Co-pyrolysis characteristics of municipal sewage sludge and hazelnut shell by TG-DTG-MS and residue analysis. Waste Manag 62:91–100

Xue GH, Gao ML, Gu Z, Luo ZX, Hu ZC (2013) The removal of p-nitrophenol from aqueous solutions by adsorption using gemini surfactants modified montmorillonites. Chem Eng J 218:223–231

Yuan X, Huang H, Zeng G, Li H, Wang J, Zhou C, Zhu H, Pei X, Liu Z, Liu Z (2011) Total concentrations and chemical speciation of heavy metals in liquefaction residues of sewage sludge. Bioresour Technol 102(5):4104–4110

Yuan H, Lu T, Zhao D, Huang H, Noriyuki K, Chen Y (2013) Influence of temperature on product distribution and biochar properties by municipal sludge pyrolysis. J Mater Cycles Waste Manage 15(3):357–361

Zhang FS, Nriagu JO, Itoh H (2005) Mercury removal from water using activated carbons derived from organic sewage sludge. Water Res 39(2):389–395

Zhao B, Xu XY, Xu SC, Chen X, Li HB, Zeng FQ (2017) Surface characteristics and potential ecological risk evaluation of heavy metals in the bio-char produced by co-pyrolysis from municipal sewage sludge and hazelnut shell with zinc chloride. Bioresour Technol 243:375–383

Zhao B, Xu XY, Li HB, Chen X, Zeng FQ (2018) Kinetics evaluation and thermal decomposition characteristics of co-pyrolysis of municipal sewage sludge and hazelnut shell. Bioresour Technol 247:21–29